Available online at www.sciencedirect.com
ScienceDirect
International Journal of Thermal Sciences 47 (2008) 963–971
International Journal of Thermal Sciences
www.elsevier.com/locate/ijts

Convective evaporation model of sessile droplets in a turbulent flow—comparison with wind tunnel data

H.K. Navaz *, E. Chan, B. Markicevic

Kettering University, Department of Mechanical Engineering, 1700 W. 3rd Avenue, Flint, MI 48504, USA

Received 11 May 2007; received in revised form 23 August 2007; accepted 27 August 2007

Available online 24 October 2007

Abstract

A semi-analytic model for convective evaporation of sessile droplets from solid surface has been developed. The effect of turbulence on evaporation is incorporated into the model through the use of the friction velocity. The friction velocity is calculated from the wall shear stress that was obtained experimentally as a function of free stream velocity and turbulence intensity. In the model, the Reynolds number based on the friction velocity was used because it is more pertinent for sessile droplets than the Reynolds number based on the free stream velocity. Thus formulated model has been successfully validated with wind tunnel data, where a very good agreement between the model predictions and experimental measurements is observed. By utilizing the model, a unique evaporation master curve that correlates the normalized evaporation mass and the non-dimensional time corrected for the influence of the driving force was developed for all droplet sizes, free stream velocities, turbulence intensities, and the surrounding temperatures.

Keywords: Sessile droplet; Convective evaporation; Turbulence effects; Dimensionless analysis

1. Introduction

The evaporation of sessile droplets is encountered in the chemical warfare. These chemicals could be extremely toxic and lethal. They start to spread into their surroundings immediately after their release. This spreading can take place in different phases and modes, i.e. liquid, vapor, adsorption, and as a solvable substance. Before an agent reaches the ground, transient evaporation is the only mechanism that controls agent's departure from its original entity. However, when the agent reaches the ground the transport mechanisms become more versatile. Adsorption, evaporation, and diffusion are the major mechanisms in the agent transport on/from the ground and below the surface. If the ground is wet the agent may be dissolved into the water causing that all transport mechanisms to follow a multi-component system governing equations. A similar problem is also encountered when pesticides are used. The evaporation of any pesticide in the liquid form will affect the quality of air and the toxicologist can predict the effects of inhaling such chemicals on body tissues.

A comprehensive evaporation model of a drop deposited on an impermeable surface with no convective effect is discussed by Popov [1]. Similar studies are performed by Hu et al. [2] who have used the finite element method to solve for the vapor concentration above the droplet. A simple evaporation model in the presence of convection is developed by Baines et al. [3] with a doubtful accuracy. In some cases an over-prediction of 90% was observed in using their model. A comprehensive literature review of the existing models is presented by Winter et al. [4]. All of the previous studies are mostly focused on capturing some of the physics of evaporation and they do not address the role of the turbulence on the evaporation. Hence, previous models lack in their ability to predict any realistic event that involves chemical agents, and a major requirement for an agent model to be scalable to outdoor conditions. That is to say to establish a method for realistic prediction of a scenario by only using the results of a limited laboratory (wind tunnel) tests.

In this study an evaporation model for sessile drops is developed and the model coefficients are determined for a chemical agent, HD (Mustard). The model takes into account the contri-

* Corresponding author.
E-mail address: hnavaz@kettering.edu (H.K. Navaz).

1290-0729/$ – see front matter
doi:10.1016/j.ijthermalsci.2007.08.004

Nomenclature

A_s	Surface area	m^2
c_p	Specific heat at constant pressure	$J\,mol^{-1}\,K^{-1}$
D	Diffusion coefficient	$m^2\,s^{-1}$
h	Height of the droplet	m
h_{fg}	Latent heat of evaporation	$J\,mol^{-1}$
m	Mass	kg
P	Pressure	Pa
Pr	Prandtl number	
r	Wetted area radius	m
R	Radius of curvature	m
Re	Reynolds number, u^*R/ν	
Sc	Schmidt number	
T	Temperature	K
V	Volume	m^3
Y	Mole fraction	
x, y	Coordinate system	
u^*	Friction velocity, $\sqrt{\tau_w/\rho}$	$m\,s^{-1}$

Greek symbols

α	Thermal diffusivity	$m^2\,s^{-1}$
β	Contact angle	
φ	$\frac{\pi}{2} - \beta$	
λ	h/r	
μ	Viscosity	Pa s
ρ	Density	$kg\,m^{-3}$
Θ	T/T_{ref}	
τ	Shear stress	Pa

Subscripts

ℓ	Related to the liquid phase
M	Related to mass transfer
s	Surface of the droplet
T	Related to heat transfer
vap	Vapor phase
V	Volume
w	At the wall
∞	Far field

Superscripts

$''$	Per unit area
$\cdot$	Per unit time

bution from the free stream turbulence and it demonstrates that the presence of turbulence can greatly increase the evaporation rate. Furthermore, a similar group for non-dimensional time is found. This group can be used to scale the laboratory test results to the outdoor conditions.

2. Analytical model development

The sessile droplet deposited on an impermeable surface is usually in the shape of a spherical cap. The droplet and its geometrical dimensions are as shown in Fig. 1(a), where the droplet is given with the base radius (r) and its height (h). The curvature of the corresponding spherical cap (R_s) is also shown. Initial geometrical values of (r_0, h_0, $R_{s,0}$) of the droplet are influenced by liquid surface tension and they are calculated from the advancing contact angle (θ_a) and the droplet volume (V_0). The angle (θ_a) is liquid/impermeable surface specific. Due to the evaporation, the droplet shrinks in size, where the surface tension again plays a major role in changes of the droplet shape in time. The retreating contact angle (θ_r) is defined, where ($\theta_r < \theta_a$) and again, it is liquid/impermeable surface specific. For the contact angle ($\theta_r < \theta < \theta_a$), the droplet base radius (r) remains constant ($r = r_0 = \text{const}$) while the droplet height (h) decreases as depicted in Fig. 1(b). Once the condition ($\theta = \theta_r$) is met, the droplet starts to shrink in both height (h) and base radius (r), but keeping angle (θ) constant and equal to ($\theta = \theta_r$) as shown in Fig. 1(c). This condition translates into $\lambda_r = h/r = \text{const}$. It should be noted that this evaporation mechanism holds for certain substances including HD that is being considered here as shown in the experimental results of Hin [5]. The formulations for cases following either or both mechanisms are derived here.

Irrespective of the evaporation mechanism ($r = \text{const}$ or $\lambda_r = \text{const}$), the instantaneous volume (V) and free surface (A_s) of a sessile droplet are given as:

$$V = \frac{1}{3}\pi h^2(3R - h) = \frac{1}{6}\pi h(3r^2 + h^2)$$
$$A_s = 2\pi Rh \tag{1}$$

Having the mass rate of evaporation ($\dot{m}$) equal to the negative change of the mass (m) left on the surface in time (t) and from Eq. (1), it can be written:

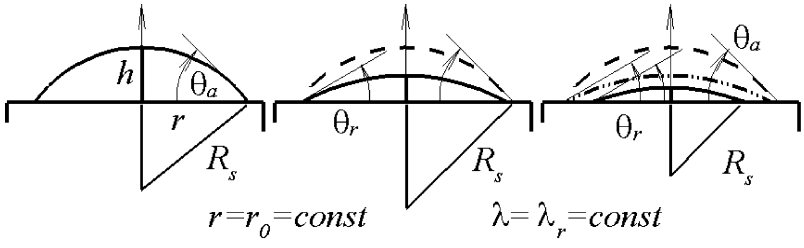

Fig. 1. Schematic of a droplet on an impermeable substrate and evaporation mechanisms, where initially droplet base radius (r_0) is constant that is followed by constant droplet height to the droplet radius ratio (λ_r).

$$\dot{m} = -\frac{\mathrm{d}}{\mathrm{d}t}m = -\frac{\mathrm{d}}{\mathrm{d}t}(\rho_\ell V) = -\rho_\ell \frac{\pi}{2}(r^2 + h^2)\frac{\mathrm{d}h}{\mathrm{d}t} \tag{2}$$

where (ρ_ℓ) is the liquid density. From Eq. (2), the height of the droplet is calculated as:

$$\frac{\mathrm{d}h}{\mathrm{d}t} = \frac{-\dot{m}}{\rho_\ell \frac{\pi}{2}(r^2 + h^2)} \tag{3}$$

The instantaneous droplet height can be obtained by integrating Eq. (3) provided that the forcing function $(\dot{m})$ is known. There are numerous expressions in the literature for the evaporation rate $(\dot{m})$ and references [6–10] list detailed derivation of $(\dot{m})$. It is shown [6] that the rate of evaporation $(\dot{m})$ can be written as a product of two functions (f_1) and (f_2) which depend on the droplet surface area $f_1(A_s)$ and transport parameters $f_2(T_p)$, respectively. This rate is modified for sessile drops where it is found that $f_1(A_s) = 2\pi\lambda R_s$ and (λ) represents the instantaneous aspect ratio (h/r) (see Fig. 1):

$$\dot{m} = f_1(A_s) f_2(T_p) = 2\pi\lambda R_s f_2(T_p) \tag{4}$$

Combining $f_1(A_s) = 2\pi\lambda R_s$ and Eqs. (3) and (4) and using geometrical condition $R_s^2 = r^2 + (R_s - h)^2$, the instantaneous droplet height can be calculated respectively for both evaporation mechanisms ($r = \text{const}$) and ($\lambda_r = \text{const}$) as follows:

$$\frac{\mathrm{d}h}{\mathrm{d}t} = -\frac{2}{\rho_\ell r_0} f_2(T_p) \quad \text{and} \quad \frac{\mathrm{d}h}{\mathrm{d}t} = -\frac{2\lambda_r}{\rho_\ell h} f_2(T_p) \tag{5}$$

The form of the transport function $f_2(T_p)$ for a droplet evaporation into quiescent surrounding is given with the transfer number (B) and for the evaporation considered as heat transfer problem $(T_{p,H})$ one can write:

$$f_2(T_{p,H}) = \rho\alpha \ln(1 + B) = \frac{\mu}{Pr}\ln(1 + B) \tag{6}$$

Where (ρ) and (μ) are the surrounding fluid density and viscosity, (α) is thermal diffusivity and the Prandtl number is defined as $Pr = \mu/(\rho\alpha)$. By using the analogy between the heat and mass transfer $(T_{p,M})$ in which the Schmidt number, $Sc = \mu/(\rho D)$ and the mass transfer number (B_M) are used, another form of the above equation can be written as:

$$f_2(T_{p,M}) = \frac{\mu}{Sc}\ln(1 + B_M) \tag{7}$$

In Eqs. (6) and (7), the heat and mass transfer numbers (B) and (B_M) are computed from the temperature (T) and the mole fraction (Y), respectively, with the values at the droplet surface (s) and the bulk constant conditions (∞) used:

$$B = \frac{c_p(T_\infty - T_s)}{h_{fg}} \quad \text{and} \quad B_M = \frac{Y_\infty - Y_s}{Y_s - 1} \tag{8}$$

and (c_p) and (h_{fg}) are heat capacity and latent heat of evaporation.

In order to calculate the transfer numbers, the temperature and the mole fraction at the droplet free surface (T_s and Y_s) need to be known. It is very difficult to perform measurements of these variables and to calculate the transfer numbers thereafter. It will be more beneficial and practical to find a functional form of the transfer numbers based on the bulk temperature and vapor pressure at the bulk temperature from the experimental data. Therefore, the transfer numbers are replaced by $\Lambda(T, Y_s)$ (representing $T = T_s = T_\infty$ and Y_s at T_∞) for the heat transfer driven equation, and by $\Omega(Y_s)$ (depending on Y_s) for the mass transfer equation. Furthermore, due to the convective nature of the evaporation, Eqs. (6) and (7) are modified to include the Reynolds number that account for the convective transport.

$$f_2(T_{p,H}) = \frac{\mu}{Pr}(F_T + C_T Re^{m_T} Pr^{n_T})\ln\big[1 + \Lambda(T, Y_s)\big] \quad \text{model 1} \tag{9}$$

$$f_2(T_{p,M}) = \frac{\mu}{Sc}(F_M + C_M Re^{m_M} Sc^{n_M})\ln\big[1 + \Omega(Y_s)\big] \quad \text{model 2} \tag{10}$$

The terms $\Lambda(T, Y_s)$ and $\Omega(Y_s)$ also need to be found, and the next functional dependencies are proposed:

$$\Lambda(T, Y_s) = \left(\frac{Y_s}{1 - Y_s}\right)^{\xi(\Theta)} \quad \text{and} \quad \Omega(Y_s) = \left(\frac{Y_s}{1 - Y_s}\right)^{1.1125} \tag{11}$$

where $\xi(\Theta) = -81.96 + 247.136\Theta - 244.75\Theta^2 + 80.4056\Theta^3$, $\Theta = \frac{T}{T_{\text{ref}}}$ (absolute temperatures in °R) and $Y_s = \frac{P_{\text{vap}}}{P}$.

The constants F_T, C_T, m_T and n_T are convective transfer constants for the first equation and F_M, C_M, m_M and n_M are constants for the second equation that need to be determined from the experimental results. The vapor pressure (P_{vap}) is calculated for the bulk temperature (T) and the exponent in $\Omega(Y_s)$ term and function $\xi(\Theta)$ are found from the experimental data. The Reynolds number is defined using a characteristic velocity (u_{charactr}) and a characteristic geometrical dimension (d_{charactr}) and it is equal to $Re = \rho d_{\text{charactr}} u_{\text{charactr}}/\mu$, where (d_{charactr}) is equal to the droplet cap curvature (R_s) (see Fig. 1). Finally, due to the turbulence effects the characteristic velocity is set equal to the wall friction velocity (u^*).

The model is now further extended to include the effect of the free stream turbulence. In the classic boundary layer theory, as the flow reaches a solid surface the velocity reduces, inertial forces are gradually diminished, and viscous effects become more dominant. On the other hand, viscous forces characterized by the wall shear stress are affected by the amount of turbulence level in the free stream. Therefore, a sessile droplet experiences both "driving forces" for its evaporation, velocity and turbulence level. It is postulated here that both effects are embedded in what is called the friction velocity ($u^* = u_\tau = \sqrt{\tau_w/\rho}$, where (τ_w) is the wall shear stress and (ρ) is the free stream density). It is also hypothesized that the effects of the free stream turbulence intensity and velocity magnitude can be incorporated into the evaporation model through using the Reynolds number based on the friction velocity rather than the usual free stream velocity. That is to say that the Reynolds number is calculated using the velocity that is "seen" by a sessile drop.

3. Results and discussions

In order to check the evaporation models developed, two series of experiments were carried out. A series of boundary

Table 1
Shear stress at the wall as a function of the free stream velocity and turbulence intensity

Free stream speed (m/s)	Turbulence intensity		
	0.3–0.4%	2.6%	4.1–5.4%
	τ_w (shear stress at the wall, Pascal)		
2	0.0249	0.0251	0.0253
5	0.0626	0.0663	0.0723
10	0.2048	0.2102	0.2483
15	0.4096	0.4450	0.5115

Table 2
The convective heat (T) and mass (M) transfer parameters

	F	C	m	n
Heat—Eq. (9)	0.1	0.07	1.0	0.25
Mass—Eq. (10)	1.	4.	1.0	0.4

layer measurements were made at the Caltech's $6' \times 6'$ wind tunnel. The turbulence intensity was altered while the mean velocity was maintained constant. Table 1 shows the wall shear stress as a function of the free stream velocity and turbulence intensity [11]. For arbitrary free stream velocity and turbulence intensity within the range in Table 1, the friction velocity (u^*) is calculated by finding the wall shear stress by interpolation from Table 1, and the free stream density is obtained from the operating temperature and pressure.

In the second group of experiments, the droplet evaporation rates were measured for varying droplet volume and free stream flow conditions. Three distinct initial droplet volumes, V_0 (μL) $= \{1, 6, 9\}$ were used. The wind tunnel tests were performed at four different free stream velocities, u_{free} (m/s) $= \{0.26, 1.77, 3.00, 3.66\}$ and the wind tunnel air temperatures were set at T (°C) $= \{15, 25, 35, 50, 55\}$. It has been experimentally observed [5] that the evaporation of HD droplets start with an initial contact angle of about $\theta_a = 28°$ and proceeds with ($r = r_0 = \text{const}$) mechanism (reducing contact angle), and then switches to ($\lambda_r = \text{const}$) at a contact retreating angle of about $\theta_r = 10°$. A numerical procedure that solves the governing equation (5) along with Eqs. (9) or (10) (including Eq. (11) for $\Lambda(T, Y_s)$ or $\Omega(Y_s)$ terms) was developed. The scheme is based on the Runge–Kutta fourth order integration algorithm. The available data for $V_0 = 1$ μL droplet at four temperatures (with $T_{\text{ref}} = 15\,°\text{C}$) and free stream velocities were used to find all the model parameters including the constants in Eq. (11) for $\Lambda(T, Y_s)$ and $\Omega(Y_s)$ functions. The turbulence intensities of 1.5%, 2.2%, 2.5%, and 2.8% were used respectively for four free stream velocities of u_{free} (m/s) $= \{0.26, 1.77, 3.00, 3.66\}$ to calculate the friction velocity (u^*). For the two models based on heat (T) and mass (M) transfer, the convective transport coefficients F, C, m and n are shown in Table 2. After finding the model constants, the numerical predictions for different set of input data, i.e., droplet size, temperature, and free stream velocity, are compared with experimental results. Furthermore, the validated model was used to perform parametric studies to understand the importance of temperature, free stream velocity, and turbulence intensity on the evaporation. The results of this study were compiled to find a similar solution for the percentage (%) of mass left (compared to initial mass) as a function of non-dimensional time. The similar solution can be scaled from the wind tunnel experiments to outdoor data.

Figure 2 shows the comparison between both models (1 and 2 in Eqs. (5), (9) and (10)) and the experimental data for $V_0 = 1$ μL droplets. It can be seen that by almost doubling the free stream velocity an increase in evaporation rate of about 25% can be achieved at the same temperature. Figure 2 also indicates that by almost doubling the temperature (15 to 35 °C) at the same velocity (1.77 m/s) the evaporation rate has become five (5) times faster. This indicates that the evaporation is more sensitive to the temperature than to the free stream velocity. At higher temperatures the main driving force for evaporation becomes the vapor pressure (P_{vap}), and therefore (Y_s).

A similar comparison is made for the available data for $V_0 = 6$ μL droplets that are exposed to the same temperature and/or free stream conditions. These results are shown in Fig. 3 and the comparison is very good regardless of the fact that all model parameters are unchanged. Investigating the changes in the evaporation time we came to the same conclusions for the influence of (u_{free}) and (T) as for droplet $V_0 = 1$ μL. The third droplet volume investigated is $V_0 = 9$ μL drops and experimental results and their comparison with numerical predictions are summarized in Fig. 4. Again, a very good agreement between experimental results and numerical predictions is observed. The influence of free stream velocity and its temperature (u_{free}) and (T) on the evaporation is the same as in the previous cases for smaller droplets. There is an under- or over-prediction when the two models are compared with experimental data. However, the faster the evaporation becomes more error can occur in measuring the vapor phase (see Fig. 4, $T = 55\,°$ case).

The previous analysis reveals that there is a difference in how the individual parameters influence the evaporation rate. It also seems that the evaporation rate is most influenced by bulk air temperature. Having the analytical formulation validated, the model can now be used for parametric studies. To do this, a small ($V_0 = 1$ μL) and large ($V_0 = 9$ μL) droplet are subjected to only one varying parameter at a time. To examine the influence of turbulence intensity on the evaporation, the free stream velocity and temperature are kept constant and the turbulence intensity has varied from 0.3 to 6%. For the highest and lowest (laminar) turbulence intensities the evaporation rate was altered by a factor of three (3) regardless of the size of the droplet. This is expected as the contribution of turbulence is accounted for in the Reynolds number raised to the same power. Figure 5 depicts this finding and emphasizes the fact that free stream turbulence is extremely important as a driving force that cannot be simply overlooked.

Similar study was performed to examine the significance of the free stream velocity on the evaporation by considering the smallest and largest droplets as shown in Fig. 6. In this study a free stream turbulence intensity of 2% with a constant free stream temperature of 35 °C was assumed. If the free stream velocity is increased by a factor of about fourteen (14), the evaporation time will decrease by a factor of about four (4). By the same token each free stream velocity can be correlated to the

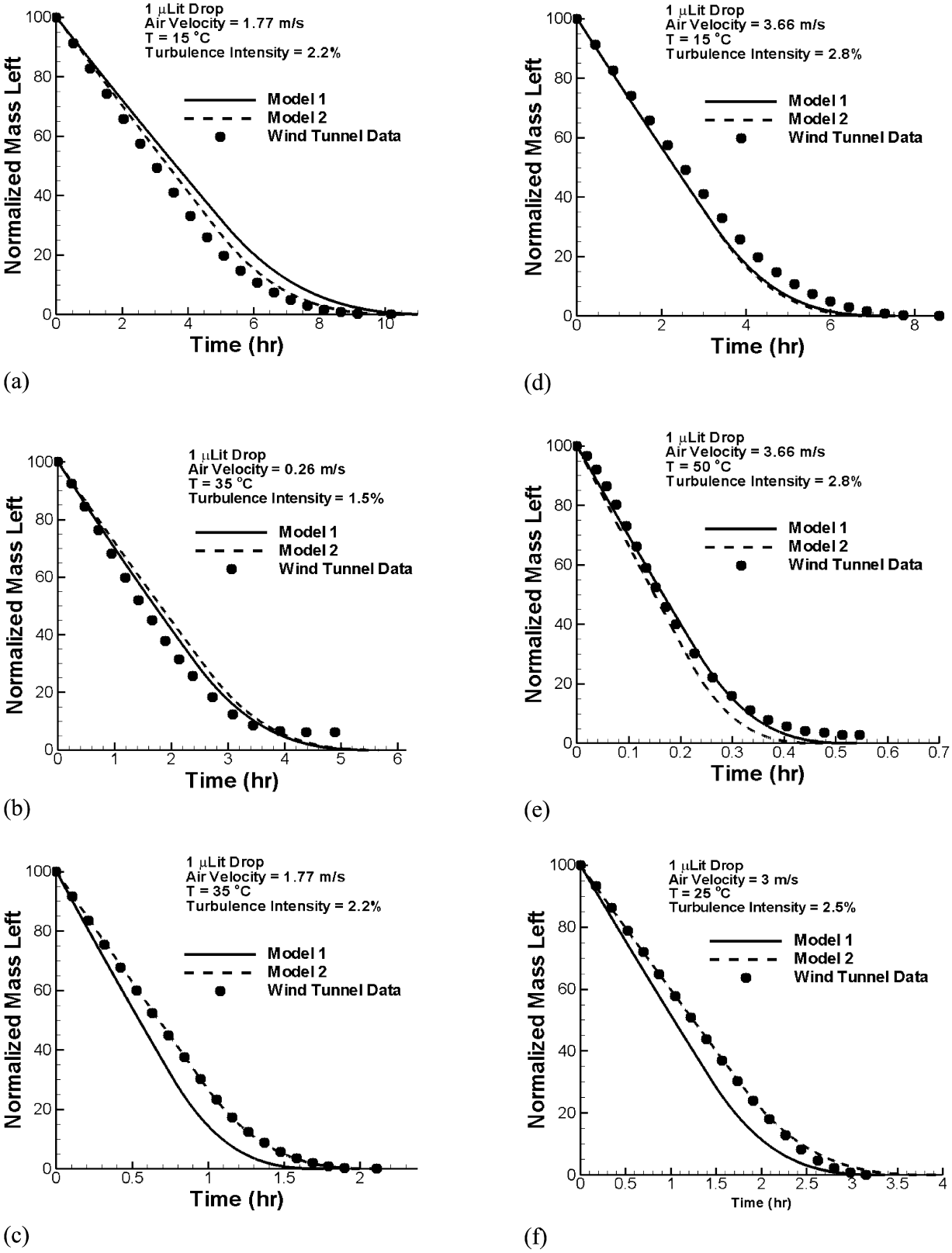

Fig. 2. Heat and mass transfer models and wind tunnel data comparison for $V_0 = 1$ μL droplet—percentage of mass left as a function of time.

evaporation time. In the last parametric study, the free stream velocity and turbulence intensity were maintained constant for the two droplet sizes and the temperature was varied. It appears that the air temperature (T) has the most significant effect on evaporation as seen from Fig. 7. For a 14% increase in absolute temperature the evaporation rate is increased by a factor of 24 due to the fact that the vapor pressure is a strong function of the temperature (the vapor pressure of HD at 30 °C is about

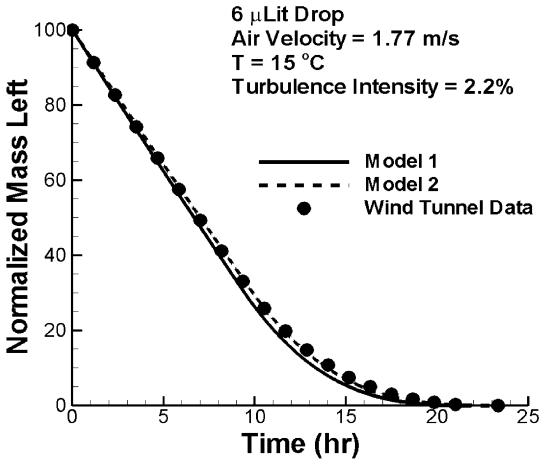

(a)

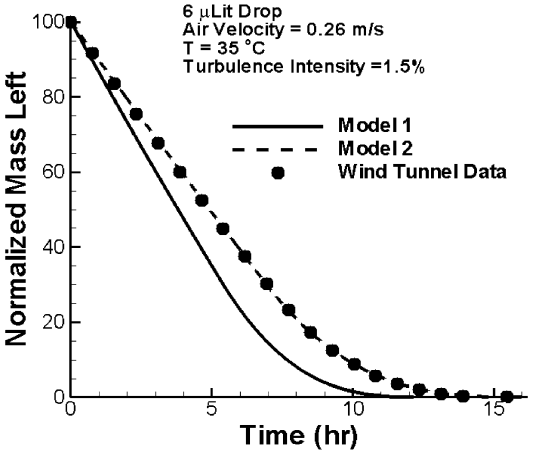

(b)

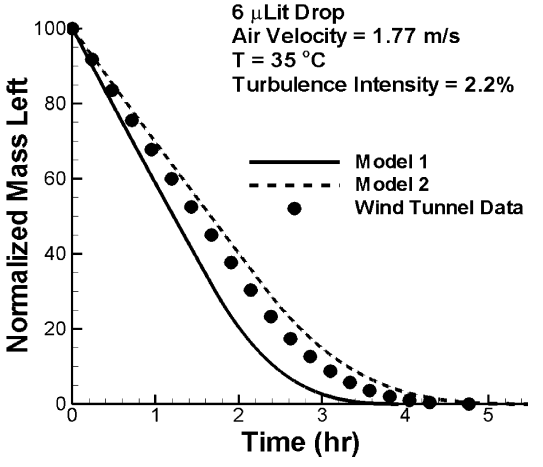

(c)

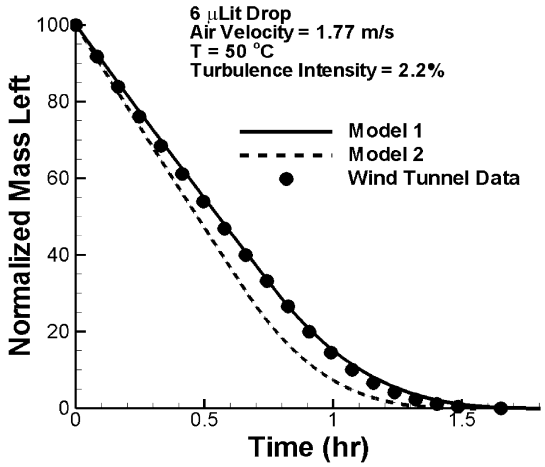

(d)

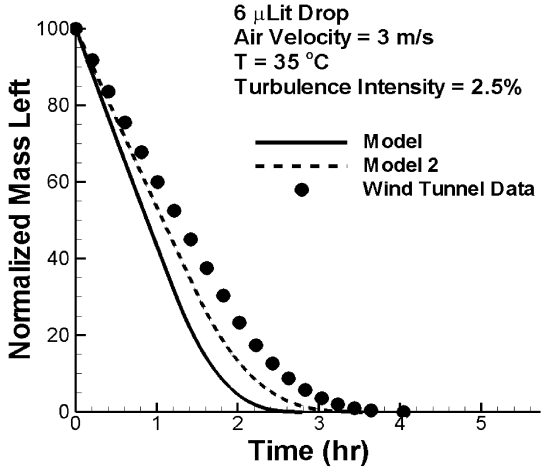

(e)

Fig. 3. Numerical and experimental wind tunnel data comparison for $V_0 = 6$ μL droplets—percentage of mass left as a function of time.

0.25 mm of Hg). On the other hand, the influence of (T) can be suppressed by increasing either (u_{free}) or turbulence intensity, thus promoting the convective transfer. Hence, two groups of the parameters can be distinguished, one that promotes driving force (temperature), and the latter ones that increase convective transfer (velocity and turbulence intensity).

3.1. Evaporation master curve

There are two major questions to be answered: (1) what is the effect of turbulence on evaporation, and (2) how do the results of wind tunnel tests can be extended to outdoor conditions. It is postulated that the friction velocity holds the answers to both questions. It was demonstrated that the friction velocity indeed can be used as a characteristic velocity to model the evaporation in turbulent flows. Using the friction velocity as a "velocity scale" combines the influences of the free stream velocity and turbulence on evaporation into a single variable. Hence, we postulate that the model should be applicable to outdoor conditions with all the calibration constants obtained in the wind tunnel. This can be done through having a good estimate of the free stream velocity and turbulence intensity and by interpolating the value of the shear stress from Table 1 and finding the friction velocity thereafter. Finally, having the evaporation model developed, there is an additional question concerning whether the evaporation curves show a single type behavior that can be reduced into an evaporation master curve.

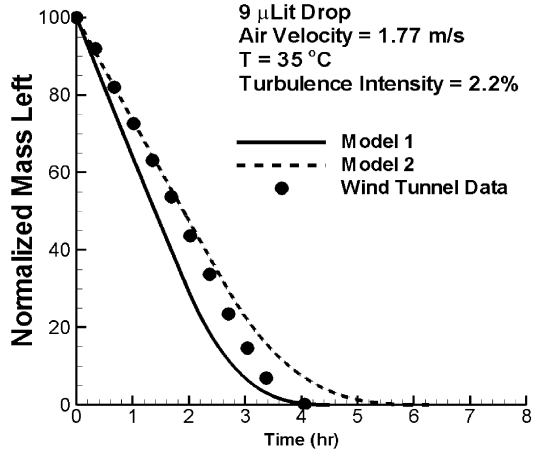

(a)

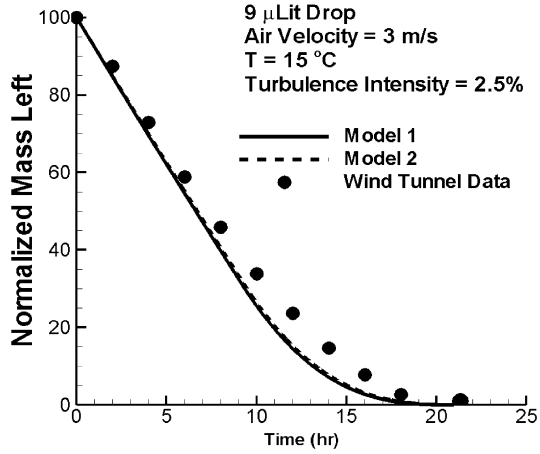

(b)

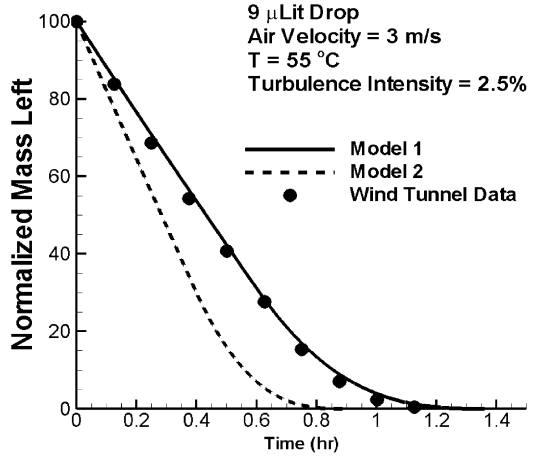

(c)

Fig. 4. Model and wind tunnel experimental data comparison for $V_0 = 9$ μL drops—percentage of mass left as a function of time.

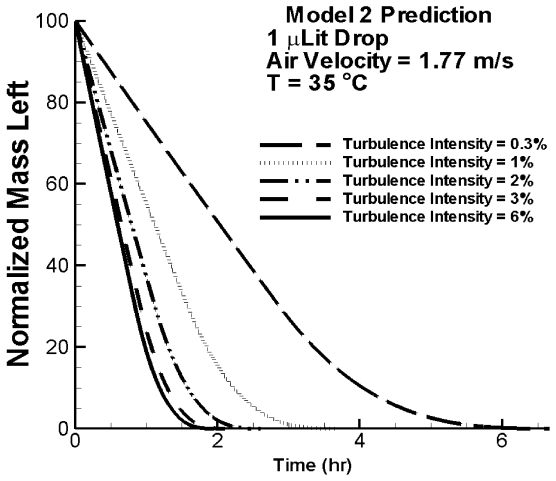

(a)

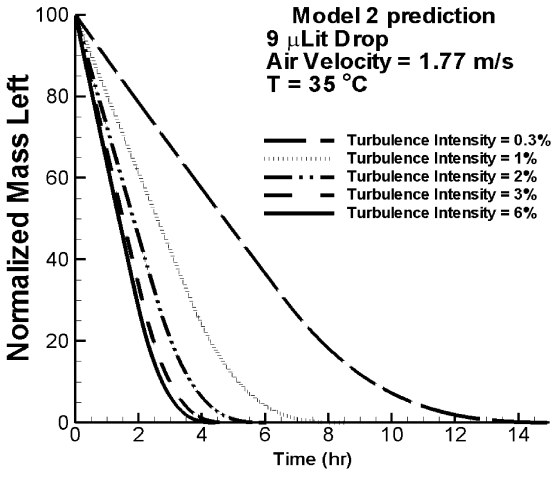

(b)

Fig. 5. The effect of turbulence intensity on evaporation.

The evaporation curves show the percentage of the initial mass left as a function of time. For the cases investigated experimentally, the evaporation time changes by two orders of magnitude (forty times), whereas the initial droplet mass (volume) changes by an order of magnitude. The models from Eqs. (9) and (10) suggest that the evaporation is influenced by: (1) geometry (because of the exposed surface to convective motion), (2) convective transfer, and (3) driving force (temperature or mole fraction). It is assumed that all three groups of parameters can be lumped into only one non-dimensional time. A geometrical factor corresponding to the transport length scale can be defined based on (V/r^2) of a droplet. The convective transport including the turbulence effects will make its contributions through the friction velocity, u^* that can be used as the velocity scale. The temperature and/or concentration gradient is accounted for through the transfer number, $\ln(1+B)$. Therefore, a similar time can be defined as:

$$tu^*(V/r^2)^{-1}\ln(1+B) = tu^*(r^2/V)\ln(1+B)$$

A similar solution for the normalized mass left should not depend on the free stream velocity, turbulence intensity, droplet size, advancing angle (type of impermeable surface), and air temperature. This assumption is confirmed against numerically generated evaporation curves by calculating the normalized

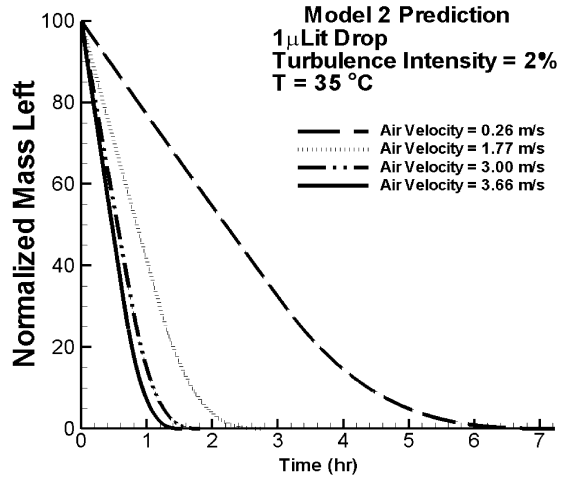

(a)

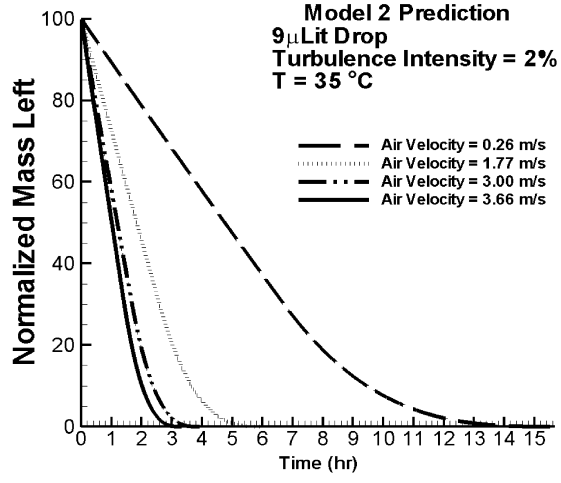

(b)

Fig. 6. The effect of free stream velocity on evaporation.

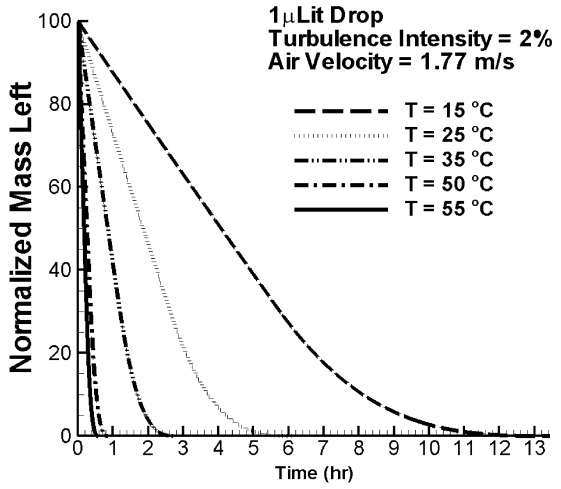

(a)

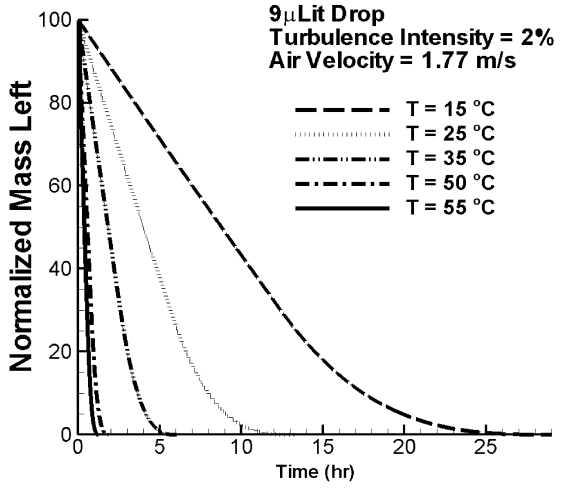

(b)

Fig. 7. The evaporation curves for different free stream temperatures.

mass left as a function of non-dimensional time for a broad range of varying droplet size with the same contact angle, free stream velocity, turbulence intensity, and temperature. The data reduction is demonstrated in Fig. 8 where the same curve is generated for all cases irrespective of the droplet size and free stream conditions. The small scatter is due to the fact that the model constants were obtained by curve fit.

The earlier hypothesis advocating the use of the friction velocity to incorporate the effects of turbulence in a scalable manner into a convective evaporation model seems to be a viable method. The curve in Fig. 8 is universal for a specific substance (HD in this work) and can be used to study the evaporation of HD droplets under the outdoor conditions as long as the friction velocity that is a boundary layer characteristic can be obtained. The change in the dynamics of the evaporation topology ($r = \text{const}$ and $\lambda_r = \text{const}$) is seen from this figure through the non-continuous gradient of the normalized mass left. This is due to a sudden change in the length scale of the similar solution. If a uniform topology change of the droplet ($r = \text{const}$ or $\lambda_r = \text{const}$) during the evaporation is assumed, the gradi-

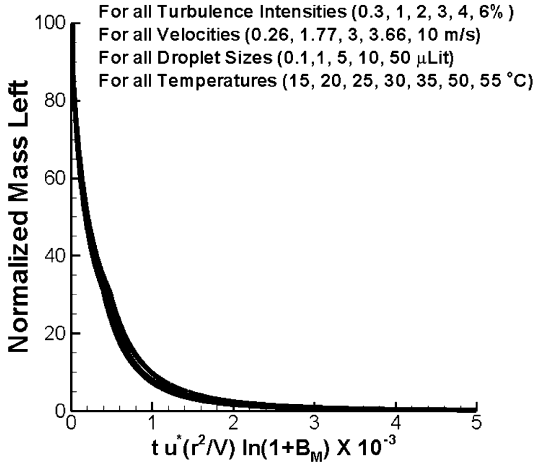

Fig. 8. Similar solutions in the form of the percentage of mass left as a function of dimensionless time that is reduced with respect to geometrical, convective and driving force parameters.

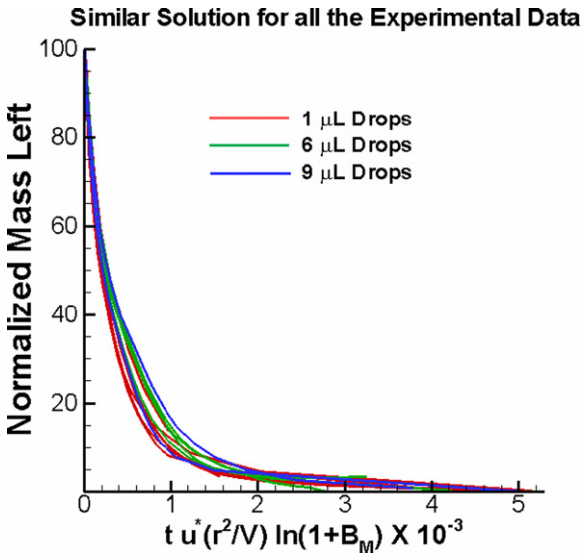

Fig. 9. Similar solutions for the available experimental data in the form of the percentage of mass left as a function of dimensionless time.

ent in Fig. 8 will remain continuous. The same similar solution was exploited to reduce all the available experimental data as shown in Fig. 9 where it is demonstrated that the experimental results follow the similar solution. To generate these curves, the amount of liquid mass left was converted to volume (V) and by knowing the contact angle and evaporation mechanism ($r = \text{const}$ or $\lambda_r = \text{const}$), the radius (r) of the wetted area was obtained. The same friction velocity and transfer number that were used to generate Fig. 8, were used to produce Fig. 9. Although, model 2 was implemented for our study, using model 1 will yield similar results and are not presented here for brevity.

4. Conclusions

Two evaporation models for sessile droplets that incorporate the effects of the free stream turbulence were developed. The models were successfully validated with available wind tunnel data for HD. The sensitivity analysis of the evaporation rate on the surrounding conditions was also carried out. These results revealed that the temperature has a major influence on the evaporation rate, but it can be altered to some extent having provided conditions of high convective transport. It was shown that the friction velocity is a suitable velocity scale for incorporating the effects of turbulence intensity level in the free stream flow. Furthermore, by using (V/r^2) as the length scale, friction velocity as the velocity scale, and natural log of the transfer number as the driving force (temperature, mass) scale, a unique master evaporation curve can be obtained. Finally, this methodology provides an important means to scale the evaporation rate of hazardous substances from laboratory tests to realistic outdoor conditions, especially due to the existing restrictions in outdoor testing of dangerous chemicals.

Acknowledgements

The authors wish to thanks the Air Force Research Laboratory, Human Effectiveness Directorate, Biosciences and Protection Division, Wright-Patterson AFB, OH, Defense Threat Reduction Agency (DTRA), and the US Army's Edgewood Chemical and Biological Center, Aberdeen Proving Ground for their support of this effort. We would like to specifically thank Dr. James Savage, Mr. William Kilpatrick, and Dr. Terrence D'Onofrio for their support throughout this project. We will also like to extend our gratitude to Dr. Art Hin of METSS for his input and most certainly examining our results throughout this work.

References

[1] Y.O. Popov, Evaporation deposition pattern: Spatial dimensions of the deposit, Physical Review E 71 (2005), Art. No. 036313-1 and 036313-17.
[2] H. Hu, R.G. Larson, Evaporation of a sessile droplet on a substrate, J. Phys. Chem. B 106 (2002) 1334–1344.
[3] W.D. Baines, D.F. James, Evaporation of a droplet on a surface, Ind. Eng. Chem. Res. 33 (1994) 411–416.
[4] S. Winter, E. Karlsson, S. Nyholm, A. Hin, Models for the evaporation of chemical warfare agents and other tracer chemicals on the ground. A literature review, Department of NBC Defense Report, S-901 82 Umea, Sweden; TNO, Prins Maurits Laboratorium, The Netherlands.
[5] A. Hin, The DREAM report: Droplet reaction and evaporation of agents model, TNO Report, 2006.
[6] K.K. Kuo, Principles of Combustion, John Wiley and Sons, New York, 1986 (Chapters 6 and 8).
[7] H.K. Navaz, A.D. Dang, The development of the liquid thrust chamber performance (LTCP) code for turbulent two-phase flow combustion of dense sprays, Technical report prepared for NASA/MSFC, Contract No. NAS8-38798, 1994.
[8] H.K. Navaz, A.L. Dang, R.H. Rangel, Numerical analysis of bipropellant combustion in liquid thrust chambers by an Eulerian–Eulerian approach, AIAA Paper No. 92-3735, 1992.
[9] J.P. Delplanque, R.H. Rangel, Droplet-stream combustion in the steady boundary layer near a wall, Combust. Sci. Tech. 78 (1991) 97–115.
[10] R.S. Miller, K. Harstad, J. Bellan, Evaluation of equilibrium and non-equilibrium evaporation models for many-droplet gas–liquid flow simulations, Int. J. Multiphase Flow 24 (1998) 1025–1055.
[11] B. Dooley, D. Jeon, M. Gharib, Boundary layer experiments and the agent fate program, Presentation by Caltech at the Chemical and Biological Defense (CBD) Conference, Baltimore, MD, 2006.